

In-Situ Multiomic Profiling of Tumor-Immune Interactions in 2D and 3D on the G4X™ Spatial Sequencer

Kenneth Gouin III, Gina Benedetto, Kaitlin Cameron, Joshua Corpuz, Ryan Costello, Sarthak Duggal, Sevana Harotoonian, Cy Hernandez, Zane Hiatt, Nathan Ing, Mark Kalaj, Andrew King, Bruna Kutche, Henry Kwan, Tung Le, Allen Lipson, Tanya McKittrick, Souad Naji, Katelyn Nelson, Rusty Nicovich, Richard Que, Florian Rath, Joseph O Ruanaidh, Jude Senarathne, Ryan Shultzaberger, Filip Shumilo, Kiera Sullivan, Ann Tong, Albert Velasco, Jessey Velasquez, Lindsay Yoo, Aubrey Zepeda, Michael Lawson, Andrew Pawlowski, Sabrina Shore, Yuji Ishitsuka, Daan Witters, Eli N. Glezer.
 Singular Genomics Systems, Inc., 3010 Science Park, Rd, San Diego, California

Introduction

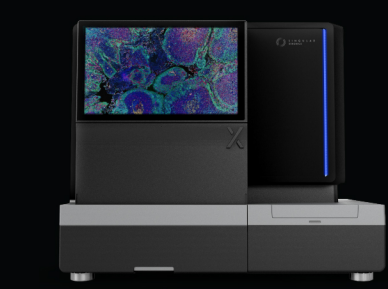
Advances in single-cell technologies have furthered our understanding of the tumor microenvironment, demonstrating that spatial context of cells is critical for understanding response to therapy. While existing spatial technologies hold promise, speed and throughput limitations restrict their applicability in translational medicine. The G4X Spatial Sequencer enables the simultaneous detection of RNA transcripts, proteins and fluorescent H&E (fH&E) staining in FFPE tissues by combining rapid 4-color SBS chemistry with high-speed, sub-micron-resolution imaging, enabling large-scale multiomic studies in cancer research.

Multiomic Profiling of Colon Normal and Cancer

FFPE samples of colon normal (n=3 serial sections) and colon cancer (n=3 serial sections) were profiled on the G4X. Multimodal (RNA + Protein) unsupervised clustering and UMAP embeddings were generated using the resulting single-cell data. Serial sections demonstrated reproducible recovery of cell types. Macrostructures revealed in the colon normal samples demonstrated the expected epithelial crypts, lymphoid patches, and smooth muscle layers, while colon cancer samples contained regions of tumor-immune interactions.

3D Reconstruction of Tumor-Normal Interface in Renal Cell Carcinoma

Ten 1cm², 5um thick serial sections of an FFPE renal cell carcinoma sample were profiled on a single G4X flow cell and serial sections were registered against each other using the fH&E images to yield a 3-dimensional reconstruction of the tumor sample. Consistent assay performance was observed across all serial sections.



Multiomics

In-situ transcriptomics, proteomics, and fH&E.

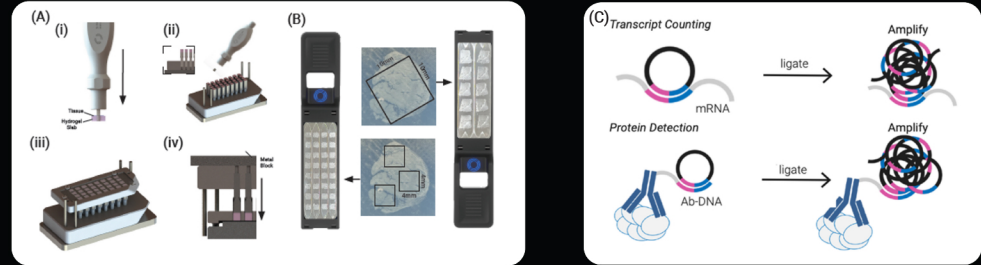
High-Throughput

40 cm² of imaging area and up to 128 samples per run.

Subcellular Resolution

Precise single-cell insights.

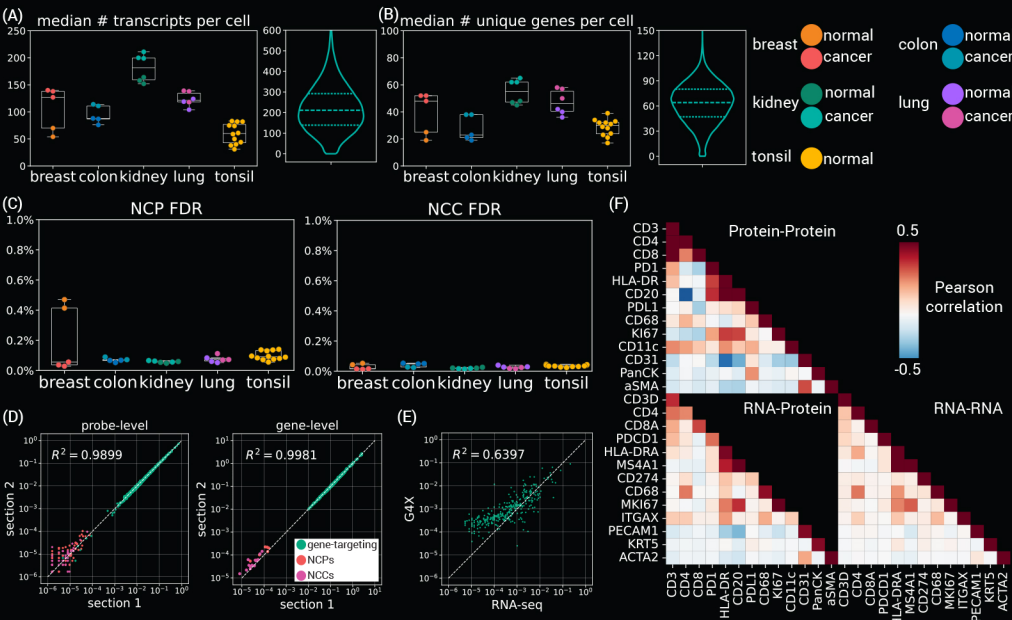
Methods



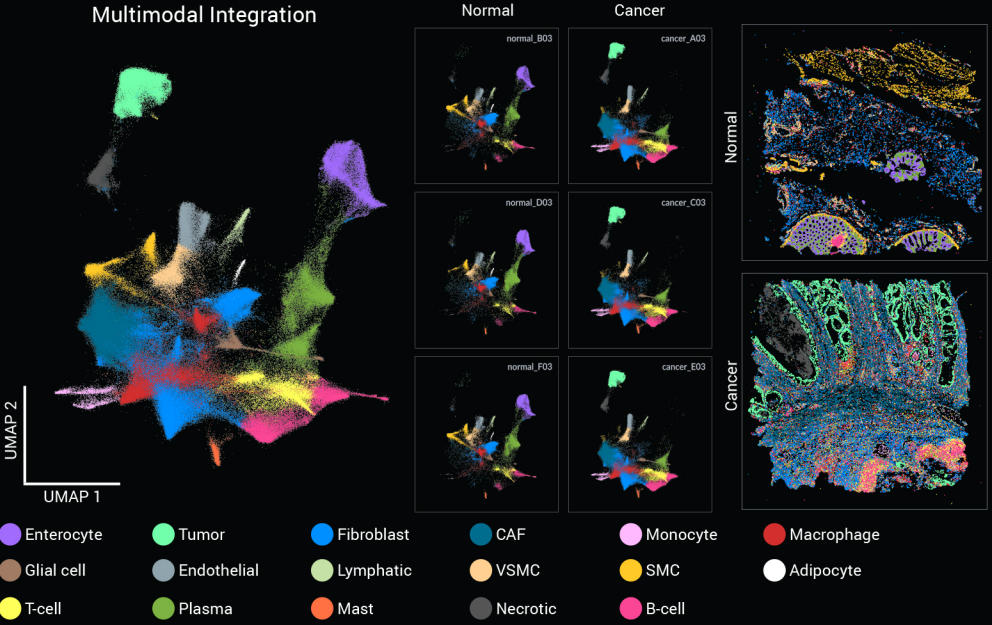
(A): Tissue Transfer Workflow: (i) A tissue section is floated on water and caught on a hydrogel slab, then a region of interest is punched with a cutter. (ii) The cutter, holding the tissue backed by hydrogel, is fitted into a pusher pillar array. (ii-insert) Cross-sectional view of the cutter loaded with tissue on a pusher pillar. (iii) A glass slide holder is aligned over the tissue array. (iv) The assembly is inverted, heat and pressure are applied to transfer the tissue onto the glass slide. (B): Examples of high-density tissue sections in flow cells (FCs), accommodating both small (4.5x4.5 mm) and large (10x10mm) sections depending on the application and tissue size. (C): In the G4X assay, transcripts are detected by hybridizing a padlock probe to a target RNA, requiring proximity of the probe's ends for ligation, enhancing specificity. Protein detection uses antibodies conjugated with oligos, targeted by padlock probes that utilize the antibody-oligo as a splint. All ligated probes are then amplified via rolling circle amplification.

Here, we demonstrate the use of 4 tissue-specific (colon, lung, kidney and breast) immuno-oncology transcript panels combined with an immuno-oncology-focused 14-plex protein panel in healthy and cancer FFPE tissue samples. Each transcript panel shares a base of ~150 immune and ~50 stromal targets complemented with ~100 tissue-specific targets. Single-cell-level data are generated using nuclear-based segmentation followed by up to 5um radial expansion constrained by neighboring cells.

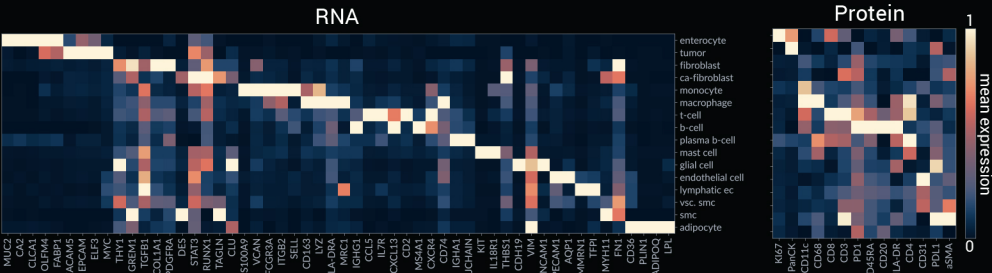
QC Metrics



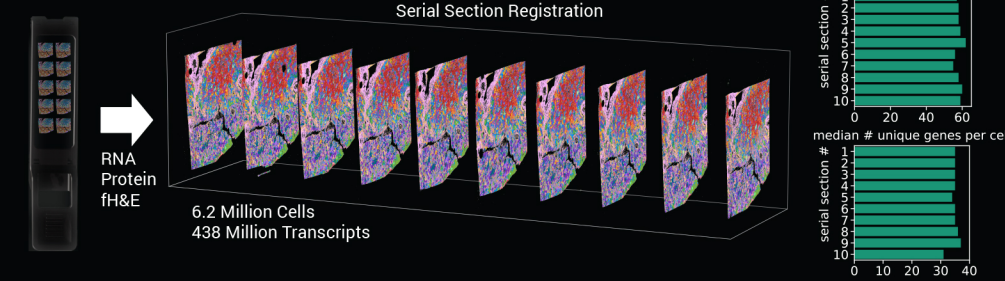
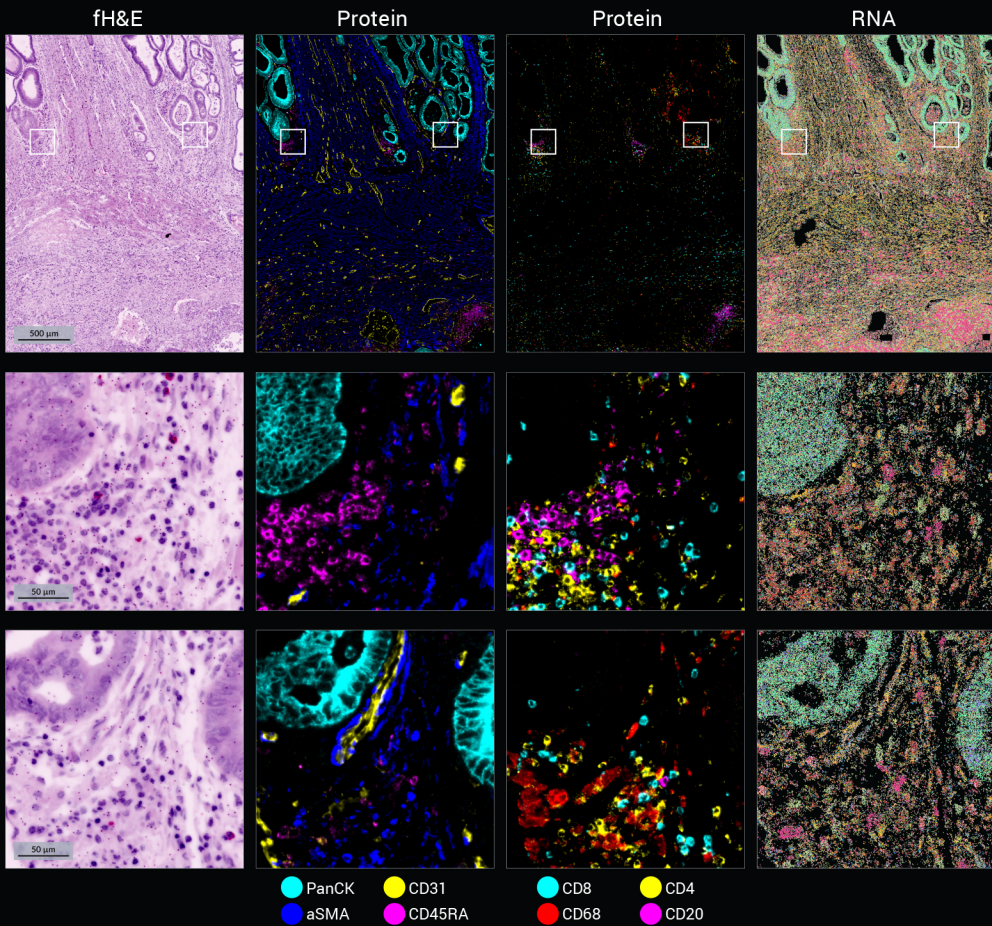
(A) Median number of transcripts and (B) unique genes per cell for each tissue type with representative violin plots showing the per-cell distribution for a single kidney cancer sample. (C) Negative control probe (NCP) and negative control sequence (NCS) false discovery rates (FDR) for each tissue type. (D) Pearson correlation of per-probe and per-gene expression between serial sections of kidney cancer profiled on two separate flow cells. (E) Correlation of gene expression between G4X and bulk RNA-seq performed on serial sections of kidney normal. Each data point represents a single gene where the total counts for each respective gene was divided by the total counts across all genes for the respective platform. (F) Pearson correlations for single-cell RNA counts and Protein mean intensities from a tonsil sample. The upper left triangle represents Protein-Protein correlations, the lower right triangle represents RNA-RNA correlations, and the lower left triangle represents RNA-Protein correlations. For the RNA-Protein correlations, the diagonal corresponds to RNA-Protein pairs, e.g. MS4A1 and CD20.



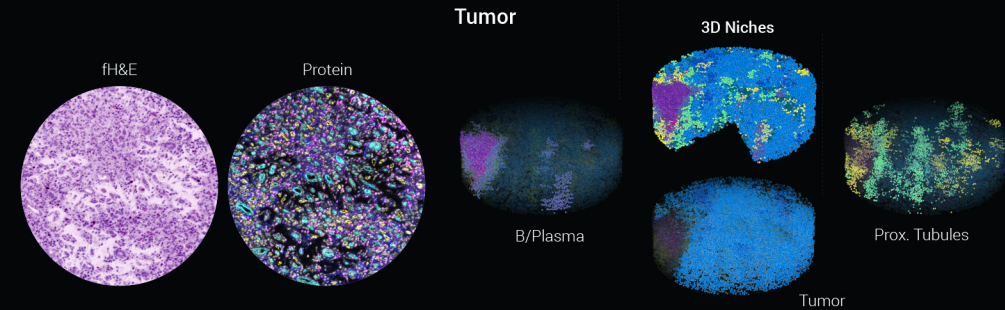
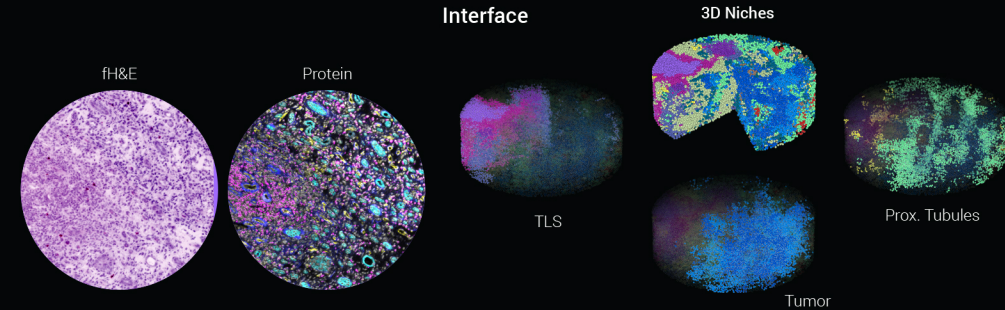
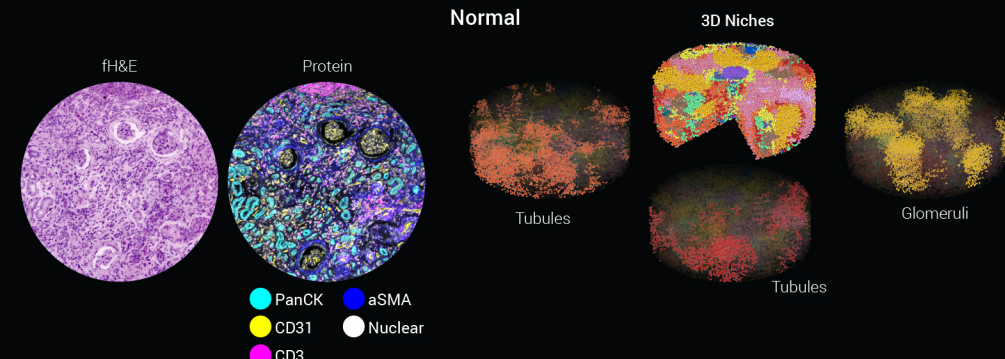
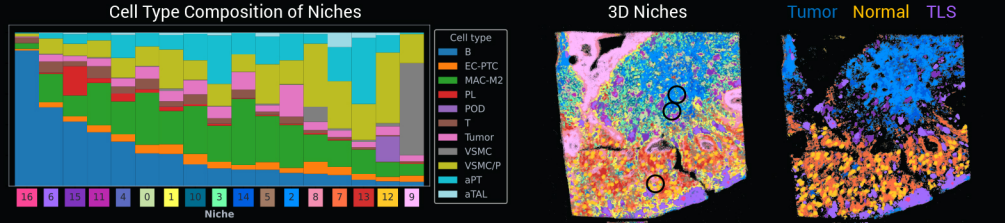
Differential gene expression analysis (logistic regression) performed on unsupervised clustering results yielded cell type profiles consistent with literature and single-cell protein expression profiles also matched expected lineage profiles.



Example macro- and micro-structure ROIs demonstrated high sensitivity and specificity across modalities. Notably, protein marker expression demonstrated the expected morphology and cellular localization. Insets marked by the white boxes in the top row are shown in the bottom two rows.



Unsupervised clustering and automated cell type annotation (CellTypist) were performed on all sections together followed by 3D spatial neighborhood (niche) detection using radii of 50um and 10um in the x/y and z axes, respectively. The recovered niches identified regions of healthy tissue (e.g. tubule niches 7 and 13 and glomeruli niche 12), cancerous tissue (niches 2 and 14), and a cancer-normal interface, which was enriched for putative tertiary lymphoid structures (TLS, niches 6, 15, and 16). Protein expression and fH&E morphology was consistent with the identified cell types in each niche. Visualization of niches in their 3D state demonstrated their continuity through the volume of the reconstruction.



Conclusion

We demonstrated high-throughput, multiomic profiling of FFPE tissues with 4 tissue-specific RNA panels in conjunction with a universal protein panel on the G4X Spatial Sequencer. G4X enables the use of different panels in each of the 2 (large format, 5cm² analyzable tissue area per lane) or 4 (small format, 1.6cm² analyzable tissue area per lane) fluidically-isolated lanes per flow cell. Utilizing this experimental flexibility, we profiled lung, breast, kidney, colon, and tonsil tissues in both normal and cancer states in a single flow cell using the 4 corresponding RNA panels and protein panel. High-quality data were produced from all tissue types with exceptional sensitivity and specificity for both modalities. In-depth analysis of colon samples demonstrated the suitability of the G4X for multimodal single-cell clustering workflows. Additionally, cell-level morphology and localization of protein expression was consistent with expectations. Finally, we leveraged the high throughput capabilities of the G4X to perform a multiomic 3D reconstruction of a renal cell carcinoma sample and utilized 3D niche detection to reveal enrichment of tertiary lymphoid structures in the cancer-normal interface.

